Investigation of thermal decomposition of yttrium–aluminum-based precursors for YAG phosphors

L. E. Muresan · E.-J. Popovici · E. Bica ·
A. I. Cadis · I. Perhaita · L. Barbu Tudoran

Abstract Three types of precursors were prepared using the wet-chemical synthesis route, starting from yttrium–europium–aluminum nitrate solution and different precipitating agents (urea, oxalic acid, and ammonium carbonate). The precursors were fired at 1200 °C in nitrogen atmosphere in order to obtain europium-doped yttrium aluminate $Y_3Al_5O_{12}$:Eu^{3+} phosphor with garnet structure (YAG:Eu). The processes involved in the thermal decomposition of precursors and their composition were put in evidence using thermal analysis (TG–DTA) and FT-IR spectroscopy. The GA–DTA curves possess typical features for basic-oxalate, -nitrate, and -carbonates as formed with oxalic acid, urea, and ammonium carbonate, respectively. Correlation between the thermal decomposition steps, mass loss, and composition of gases evolved during the thermal treatment was established using TG–DTA–FT-IR coupling. It was found that the different composition of precursors reflects on the luminescent characteristics of the corresponding phosphors. Urea and ammonium carbonate lead to the formation of YAG type phosphors, with garnet structure and specific red emission. As for the oxalic acid, this precipitating agent generates a non-homogeneous powder that contains yttrium oxide as impurity phase. This phosphor is a mixture of Y_2O_3:Eu^{3+}, $Y_4Al_2O_9$:Eu^{3+}, and $Y_3Al_5O_{12}$:Eu^{3+} that explain the relative higher emission intensity.

L. E. Muresan (✉) · E.-J. Popovici · E. Bica ·
A. I. Cadis · I. Perhaita
Raluca Ripan Institute for Research in Chemistry, Babes-Bolyai University, Fântânele 30, 400294 Cluj-Napoca, Romania
e-mail: laura_muresan2003@yahoo.com

L. B. Tudoran
Electronic Microscopy Centre, Babes-Bolyai University,
400028 Cluj-Napoca, Romania

Introduction

Inorganic phosphors have been studied extensively for use in lighting technology and manufacture of advanced display such as plasma display panel (PDP), vacuum fluorescent display (VFD), field emission display (FED), lightening emitting diode (LED), and tricolor fluorescent lamps. For enhancing the brightness and resolution of these displays, it is important to develop phosphors with high-quantum efficiency, controlled particle morphology and size [1, 2].

Yttrium-aluminum garnet $Y_3Al_5O_{12}$ (YAG) doped with various rare earth ions (Eu, Tb, Er, Ce, Sm Nd, or Pr, etc.) is one of the most important material that have been used in various application domains due to its superior mechanical stability, low thermal expansion, low acoustic losses, and excellent optical properties [3–5]. For example, doping of YAG with Nd^{3+} and Ce^{3+} leads to the construction of dye lasers and new generation lighting devices [6, 7]. Activation of YAG with Eu^{3+} generates phosphor powder or thin films used in cathode ray tube and also with potential for application in field emission devices [8, 9]. Necessary condition for optimum performance in all these devices are referring to the developing of ultrafine phosphor particles with high emission intensity [10, 11].

In the last decade, the synthesis of YAG type phosphors was performed using several methods such as: precipitation [12], sol–gel technology [13], combustion [14, 15], and spray-pyrolysis [16]. This paper is focuses on the preparation of some europium-doped yttrium aluminate YAG:Eu samples, using the wet-chemical synthesis route (precipitation)

via the simultaneous addition of reactants technique, WCS-SimAdd [17, 18].

Three types of precursors were prepared using WCS-SimAdd route starting from yttrium–europium–aluminum nitrate solution and different precipitating agents (urea, oxalic acid, and ammonium carbonate). The precursors were fired in order to obtain europium-doped yttrium aluminate $Y_3Al_5O_{12}:Eu^{3+}$ phosphor with garnet structure (YAG:Eu).

The aim of the study is to give a better understanding of the processes that take place during the thermal decomposition of the precursors. Therefore thermal analysis correlated with gas evolved analysis, FT-IR and BET investigations was performed. In addition, the paper puts in evidence the role of the precipitating agent on the morpho-structural and luminescence characteristics of yttrium-aluminate phosphors.

To the best of our knowledge, no investigation using evolved gas analysis was performed in order to highlight the possible processes that occur during decomposition of precursors for the synthesis of yttrium-aluminate phosphors.

Experimental

Europium-activated yttrium-aluminate phosphors (YAG:Eu) were prepared using wet-chemical synthesis route by simultaneous addition of reactants (WCS-SimAdd) [17] from different types of precipitating agents such as: urea (sample code EAG1); ammonium carbonate (sample code EAG14) or oxalic acid (sample code EAG15). For this purpose, Y–Al–Eu precursors were prepared from $Y(NO_3)_3 \cdot 5H_2O$ (99.9% Aldrich); $Al(NO_3)_3 \cdot 9H_2O$, (Merck); $Eu(NO_3)_3 \cdot 5H_2O$ (extra pure Merck) as metallic ion sources and urea (99.3% AlphaAesar); ammonium carbonate (PA, NH_3 25%, Chimopar) and oxalic acid dihydrate (98% Alpha Aesar) as anion source.

The synthesis of YAG:Eu was carried out in two stages. First stage was the synthesis of the Y–Al–Eu precursors by precipitation at 80 °C and pH 8 (kept constant with addition of ammonia) from equal volumes of yttrium–aluminum–europium nitrate solution (0.5 M) with urea (2 M), ammonium carbonate (0.75 M), or oxalic acid (0.75 M), which were simultaneously added into a diluted solution (1:10) of corresponding precipitating agent. The nitrate solution mixture contains Y^{3+}, Eu^{3+}, and Al^{3+} in stoichiometric amounts, corresponding to the molar ratio Y:Eu:Al = 2.97:0.03:5. The precursor post precipitation stage consisted in 24 h aging, washing, centrifugation, and drying. The second stage of the method was the thermal treatment of the precursors that was carried out at 1200 °C, in N_2 atmosphere, for 2 h. The as obtained phosphor powders were water washed, dried, and sieved; no ball milling was used during the phosphor processing. The phosphors EAG1.1, EAG14.1, and EAG15.1

were obtained from the corresponding precursor namely EAG1, EAG14, and EAG15.

Precursors were investigated by: thermogravimetric and differential thermal analysis (METTLER TOLEDO TGA/SDTA851; platinum crucible, heating rate 10 °C/min; nitrogen flow 30 mL/min); evolved gas analysis (Thermo Scientific Nicolet 6700 FT-IR Spectrometer equipped with TGA module, working at 150 °C; HR Nicolet TGA Vapor phase library), Fourier-Transform infrared absorption spectroscopy (Thermo Scientific Nicolet 6700 FT-IR Spectrometer; KBr pellet technique); surface area measurements (TriStar II3020—Micromeritics, nitrogen adsorption at 77 K, sample decontamination at 150 °C for 24 h in nitrogen flow) and scanning electron microscopy (JEOL–JSM 5510LV Microscope; Au-coated powders). The characterization of phosphors was performed by X-ray diffraction (BRUKER D8 Advance X-ray diffractometer, 40 kV, 40 mA, $\lambda_{CuK\alpha1} = 1.54056$ Å) and photoluminescence measurements (JASCO FP-6500 Spectrofluorimeter Wavel; Glass filter WG 320).

Results and discussion

To determine the influence of the precipitating agents on the morpho-structural and photoluminescence characteristics of YAG:Eu phosphor, three types of Y–Al–Eu precursors were prepared by SimAdd technique, namely EAG1(urea), EAG14 (ammonium carbonate), and EAG15(oxalic acid). After the thermal treatment of the precursors, phosphor samples with general formula $Y_{2.97}Eu_{0.03}Al_5O_{12}$ were obtained.

The precursors composition was determined by thermal analysis and IR-spectroscopy. Correlation between thermal decomposition steps, mass loss, and composition of gases evolved during the thermal treatment of the precursors was established using coupling TG–FT-IR technique. Characteristics of precursors powders were compared with corresponding phosphors samples using specific investigations.

The thermal analysis gives information on the transformations that occur during the thermal treatment from 25 to 1,200 °C. Figure 1 shows the TG and DTA curves for precursors prepared with different precipitating agent. TG curves show that the mass loss at 1,200 °C is situated between 41.3 and 57.3% meanwhile the DTA curves put in evidence the thermal effects of the main steps. The decomposition stages of sample EAG15 (oxalic acid) are very well defined with sharp endothermic peaks in comparison with EAG14 (ammonium carbonate) and EAG1 (urea) precursors. Insignificant mass loss (between 0.4 and 2.5%) is observed at temperatures above 800 °C.

Depending on the nature of the precipitating agent, the TG curves possess at least three distinct mass loss stages. The first stage occurs in the temperature range of

25–160 °C with a mass loss of 7.5% (EAG1), 11.2% (EAG14), and 2.3% (EAG15). The second stage occurs in the temperature range of 160–260 °C with a mass loss of 13.3% (EAG1), 15.1% (EAG14), and 5.6% (EAG15). The main decomposition phase for sample EAG15 takes place between 260 and 450 °C with a sharp and significant mass loss of 46.6%.

The above mentioned transformation can be ascribed to the following processes: (a) elimination of physical adsorbed water, which takes place between 50 and 150 °C, (b) elimination of chemical bonded-water, which takes place between 200 and 300 °C (sample EAG14, EAG1, EAG15), (c) decomposition of oxalate-based group, which takes place between ~300 and 450 °C (sample EAG15), (c) decomposition of basic-carbonate or basic-nitrate compounds, which takes place between 250 and 500 °C (sample EAG14, EAG1), (d) decomposition of carbonates or oxicarbonates above 700 °C (sample EAG15).

The endothermic peaks (DTA plots) situated in the temperature domain between 70 and 200 °C are associated with the removal of the moisture absorbed on the surface of particles, which takes place in two distinct stages (EAG 1, EAG 15) or in one broad step (EAG 14). The small exothermic peak at 931 °C (EAG1) is related to crystallization and crystal growth of YAG [19, 20].

It is very difficult to describe the reactions that occur during the precipitation process due to the formation of a various anionic species in the hydrolysis of the precipitating agents (CO_3^{2-}, OH^-, HCO_3^-, NH_4^+, $C_2O_4^{2-}$). One can assume that metallic ions can form, hydroxides, basic carbonates, carbonates, oxalates, and ammonia containing compounds. The competition between the reactions of the metallic ions and the hydroxyl and carbonate species from the precipitation medium gives the real composition of the precursors.

Evolved gas analysis provides additional information referring to the processes that occur during the conversion of the precursors into corresponding phosphors.

Figure 2 presents the DTG curves associated with the total infrared absorbance profiles (Gram–Schmidt curve) of gases, as function of time. FT-IR profile of gas evolved at different times is also depicted, the absorbance being normalized in relation with the strongest IR signal. Standardized notation of the ratios of CO_2 band absorbance registered at 20′, 30′, 42′ and 85′ for the three precursors are different as follows: 0.54:1:0.68:0.08 (EAG1), 0.49: 0.74:1:0.38 (EAG14), and 0.017: 0.117:1: 0.085 (EAG15).

The main decomposition stage is accompanied by a major release of gas that occurs between 200 and 400 °C (EAG1, EAG14) and 350–450 °C (EAG15), respectively. It can be seen that, the temperature of IR absorbance peaks (Gram–Schmidt curve) coincide with that weight-loss maxima (DTG plot).

The main gaseous products evolved during the thermal treatment of the precursors are CO_2, NH_3, H_2O, N_2O, NO_2, and CO easily identified by their characteristic absorbance: $v_{CO} \sim 2358$ cm^{-1} for CO_2; $\delta_{N-H} \sim 965$, 930 cm^{-1} for NH_3; v_{O-H} 3400–4000 cm^{-1}, δ_{O-H} 1300–1900 cm^{-1} for H_2O; v_{NO} 1270–1298 cm^{-1}, 2210–2240 cm^{-1} for N_2O, v_{NO} 2890–2920 cm^{-1}, 1600–1630 cm^{-1} for NO_2; v_{CO} 2181, 2112 cm^{-1} for CO.

In the temperature range of 150 ÷ 250 °C the released gas consists of ammonia (EAG1), water (EAG1, EAG14, EAG15), or carbon dioxide (EAG1, EAG14, EAG15). The elimination of CO_2 at such a low temperature indicates the decomposition of hydroxide carbonate compounds. The simultaneous release of NH_3, CO_2, and H_2O (EAG1) suggests that, during the precipitation, compounds with complex composition that contains ammonium hydroxide carbonates are formed [21].

As the thermal treatment continues and the temperature increases, all the precursors release simultaneously carbon dioxide and small amounts of water (FT-IR spectra at minute 30, 325 °C), due to the decomposition of the metallic basic carbonates. Traces of ammonia are still observed for sample EAG1. In addition, new specific bands appear and are attributed to the nitrous oxide release (metallic nitrates decomposition). At the minute 42 (445 °C) the characteristic absorbance of H_2O becomes stronger than that of CO_2 (samples EAG1 and EAG14).

Fig. 1 TG and DTA curves for precursors prepared with different precipitating agent: EAG1 (urea), EAG14 (ammonium carbonate), and EAG 15 (oxalic acid)
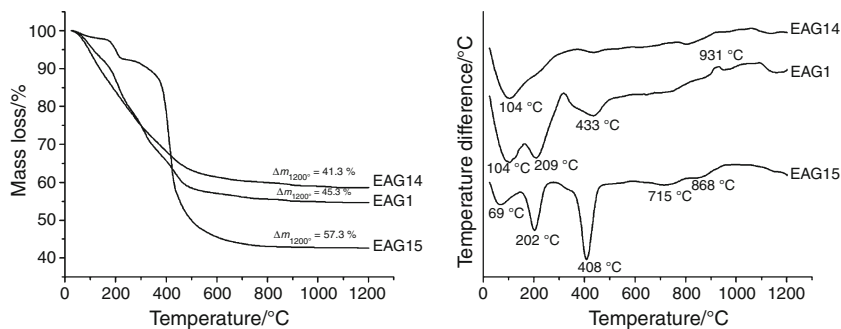
This behavior suggests that the main process is the decomposition of metallic hydroxides. Traces of nitrogen dioxide are still observed for EAG1 and EAG14. At this stage we can say that the decomposition of metallic nitrates is approaching to the completion. As for the EAG15 (oxalic acid), a massive gas release consisting mainly from CO_2 and CO is observed. This behavior suggests that the main component of the EAG15 precursor is metallic oxalates. Traces of ammonia and water are also observed, thus suggesting the decomposition of small amounts of ammonium oxalate. At 875 °C all precursors eliminate CO_2 as a result of carbonate decomposition.

The thermal decomposition of yttrium–aluminum-based precursors for YAG phosphors was further investigated using FT-IR spectroscopy, surface area measurements (BET), and scanning electron microscopy (SEM). Phosphors, the final products of the thermal decomposition process, were characterized by luminescence spectroscopy.

FT-IR spectroscopy was performed both for the precursors and the corresponding phosphor powders obtained after the thermal treatment. The FT-IR spectra confirm that the nature of the precipitating reagent directly determines the precursor composition (Fig. 3).

The precursors vibrational spectra contain some characteristic bands: $v_{as}(C=O) \sim 1,635$ cm^{-1}, $v_s(C=O) \sim 1,748$ cm^{-1}, and $v_s(C–O) + \delta(O–C=O) \sim 1,324$ cm^{-1} (EAG15); $v(NO_3) \sim 1,384$ cm^{-1}, $v(C=O) \sim 1,661$ and 1,353 cm^{-1}, $\delta(O–H) \sim 1,069, 1,160, v(Y–O) \sim 603$ cm^{-1} (EAG1); and $v(H–O) \sim 3,427$ cm^{-1}, $v_{as}(C=O) \sim 1,635$ cm^{-1}, $v(CO_3) \sim 1,528$ cm^{-1}, $v(NO_3) \sim 1,384$ cm^{-1}, $\delta(O–H) \sim 1,069$ cm^{-1}, $v(Y–OH) \sim 844$ cm^{-1} (EAG14).

After the thermal treatment, the specific bands of the precursors disappear. The bands situated at 786, 720, 690, 565, and 512 cm^{-1} are characteristic for M–O vibration and indicate the formation of $Y_3Al_5O_{12}$ crystallites [22, 23]. The FT-IR spectra put in evidence that the composition of EAG15.1 is significantly different from that of EAG1.1 and EAG14.1 phosphor samples. This suggests that, during the precipitation process, oxalic acid forms some complex species of $[Al(C_2O_4)_3]^{3-}$ type. This can lead to deviation from the stoichiometric ratio between Y^{3+} and Al^{3+} and therefore, some secondary phases can appear in the calcined powder.

Fig. 2 Gram–Schmidt diagram coupled with DTG curve (*left*) and normalized FT-IR spectra of gas evolved during the thermal treatment of precursors at different firing times (*right*)
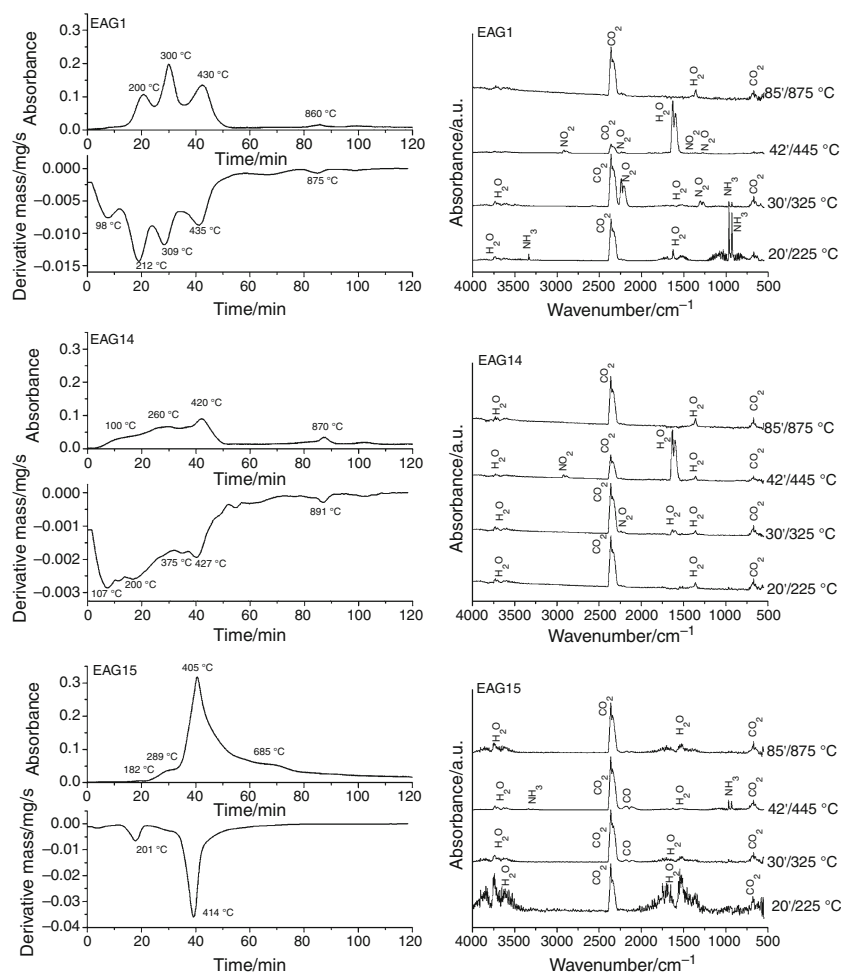
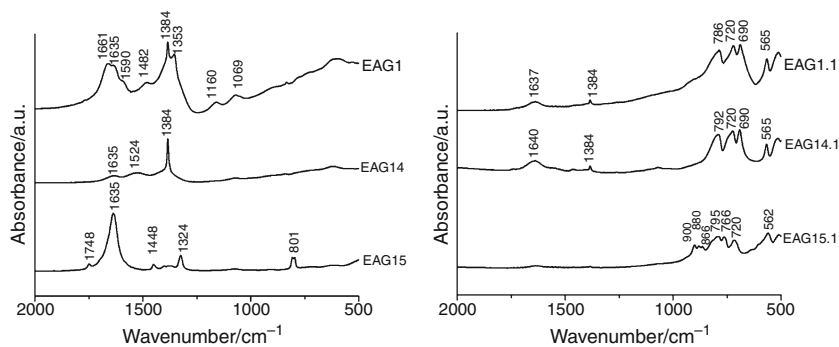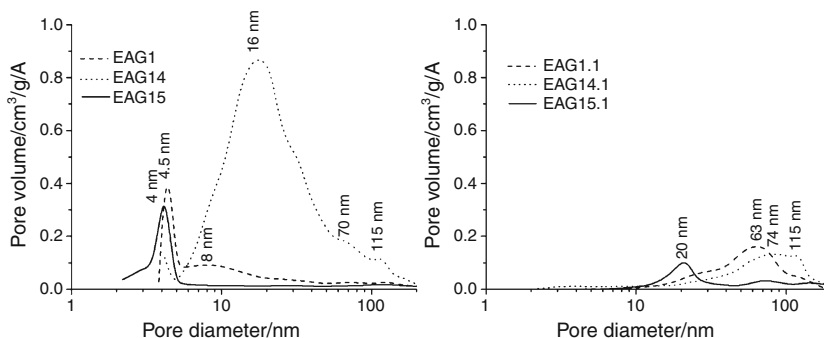**Fig. 3** FT-IR spectra for precursors (*left*) and phosphors (*right*)

Fig. 4 Pore distribution curves for precursors (*left*) and EAG phosphors (*right*)

FT-IR spectroscopy confirms the complete conversion of Y–Al–Eu precursors into europium-activated yttrium aluminate phosphors for the samples EAG1.1 and EAG 14.1.

According to the FT-IR spectroscopy associated with thermal and gas evolved analyses yttrium–aluminum-based precursors have the following general formulas: $M_2(C_2O_4)_3 \cdot a(NH_4)_2C_2O_4 \cdot bM(OH)_3 \cdot cH_2O$ (sample EAG15), $M_2(CO_3)_3 \cdot aM(OH)_3 \cdot cM(NO_3)_3 \cdot dH_2O \cdot eNH_3$ (sample EAG1), and $M_2(CO_3)_3 \cdot a M(OH)_3 \cdot bH_2O$ (sample EAG14).

Surface area measurements (BET—Brunauer, Emmett, Teller method) was performed in order to illustrate the change of surface area (S_{BET}) during the thermal treatment for all samples.

The precursor EAG14, EAG15, and EAG1 possess a surface area of: 102.39, 62.41, and 27.14 m^2/g, respectively. After the thermal treatment, the values of the surface area decrease dramatically, namely 13.87 m^2/g (EAG 14.1), 6.41 m^2/g (EAG15.1), and 7.17 m^2/g (EAG1.1). This behavior confirms once again the transformation of precursors and formation of new oxidic compounds.

BJH analysis (Baret, Joyner, and Halenda method) was used to determine area and volume of the mezo and macropores using adsorption and desorption techniques. The pore-size distributions of precursors and phosphors are compared in Fig. 4. It is obvious that, the thermal treatment leads to a significant increase of pore diameter together with decrease of their volume. Powder EAG14 (ammonium

carbonate) contains mainly mezopores that after the firing stage, is changing into macropores, with a broad distribution. Powders EAG1(urea) and EAG15 (oxalic acid) consist also of mezopores, but their dimension is about four times smaller than EAG14. The thermal treatment increases the pore dimension toward macro-domain for EAG1.1, and remains in the mezo-domain for EAG15.1.

Scanning electron microscopy (SEM) images in Fig. 5 illustrate that the precursors are powders formed from more or less porous grains with irregular shape that consist from tightly packed under-micron spherical particles (10–20 nm). The thermal treatment leads to a slight increase of the size of the sub-micron particles, making them regular and spherical.

Photoluminescence of red emitting $Y_3Al_5O_{12}$:Eu^{3+} phosphors was evaluated on the basis of emission spectra. Emission intensity of the phosphors depends on the nature of the precipitating agent as can be seen in Fig. 6.

Emission spectra present the bands due to the $^5D_0-^7F_J$ ($J = 0–5$) transitions of the Eu^{3+} ion and are situated at 588, 594, 609, 613, and 631 nm [24, 25]. It is known that in the cubic YAG phase the luminescent intensity is concentrated mainly on the $^5D_0-^7F_1$ magnetic dipole transition (~ 590 nm) rather than the $^5D_0-^7F_2$ forced electric dipole transition (~ 606 and ~ 628 nm) [24, 26]. In our case, the most intense peak (samples EAG1.1 and EAG14.1) is associated to the allowed magnetic dipole $^5D_0-^7F_1$ transition (594 nm) [24, 26]. The strongest peak for sample EAG15.1 is associated to the $^5D_0-^7F_2$

Fig. 5 SEM images for yttrium–aluminum precursors (*left*) and corresponding phosphors (*right*)
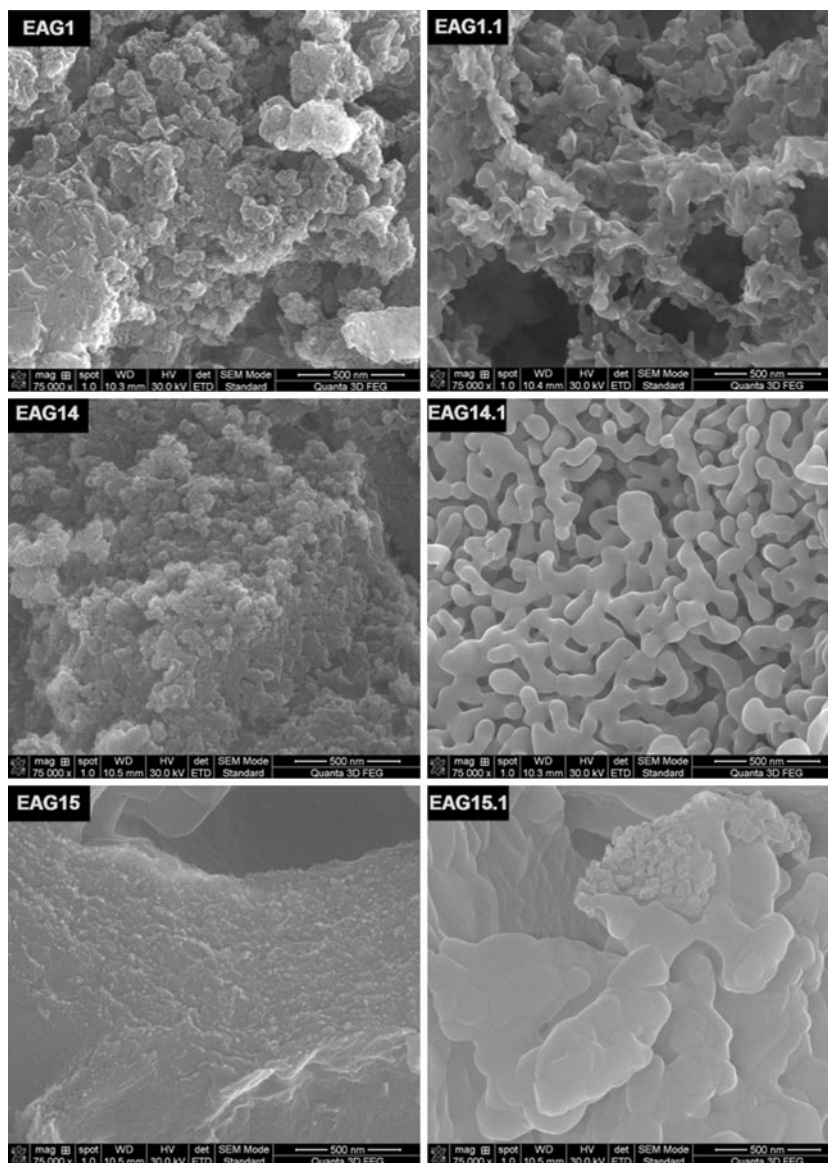
transition (613 nm) [27, 28]. This spectral data suggests that the use of oxalic acid leads to the formation of a mixture of Y_2O_3:Eu^{3+}, $Y_4Al_2O_9$:Eu^{3+} (YAM), and $Y_3Al_5O_{12}$:Eu^{3+} (YAG) and therefore the incorporation of europium ions is done differently than the other samples [29]. The XRD investigations confirmed also that the sample EAG15.1 is formed mainly of cubic Y_2O_3 ($2\theta = 29.05$; PDF25-1105) [29, 30], together with $Y_4Al_2O_9$ ($2\theta = 29.52$; PDF83-0935) [29, 31] and $Y_3Al_5O_{12}$ ($2\theta = 33.4$; PDF079-1892) [24] phases.

Figure 6 shows that emission spectra are different in terms of intensity, position and ratio of bands. The position of the strongest emission band depends on the precipitating conditions and is centered at 613 nm for EAG15.1 (oxalic acid) and at 594 nm for EAG1.1 (urea)

and EAG14.1 (ammonium carbonate). Moreover several new bands are observed in the range 400–550 nm for the sample EAG15.1. We assume that the differences in the relative intensities of the emission bands is the result of the way in which europium ions are incorporated in the host lattice, closely related with the composition of the precursor, and also to the crystallinity and phase purity of the phosphor. It is possible that the oxalic acid to facilitate the precipitation of yttrium compounds in detriment of aluminum and thus leading to the formation mainly of yttrium oxide. It is also possible that the high intensity of the band located at 613 nm to be explained due to overlapping of both $^5D_0-^7F_2$ transition in Eu^{3+} incorporated in Y_2O_3 and $Y_4Al_2O_9$ phase, respectively.
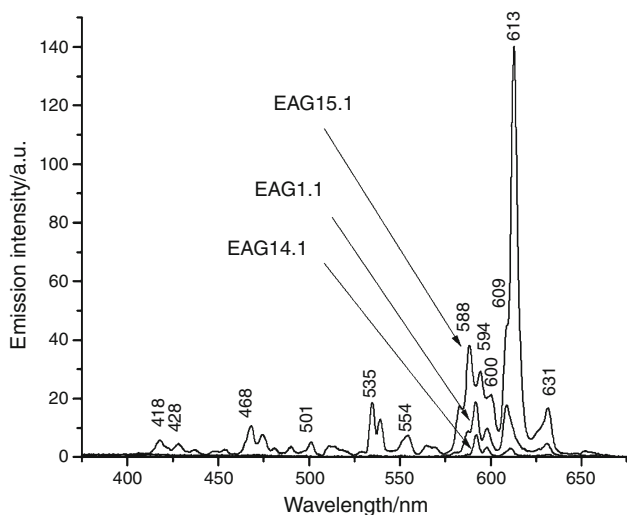
Fig. 6 Emission spectra for phosphors prepared with different precipitating agent ($\lambda_{ex.} = 254$ nm)

Conclusions

Yttrium–aluminum-based precursors were precipitated with urea, ammonium carbonate, and oxalic acid using wet-chemical synthesis route by simultaneous addition of reactants.

The thermal analysis correlated with gas evolved analysis enabled us to put in evidence the processes that take place during the thermal treatment of the precursors for the synthesis of YAG:Eu phosphors. The weight loss of the precursors varies between 41.3 and 57.3 % and occurs in at least three decomposition stages, depending on the nature of the precipitating agent. The main decomposition stage of the precursors is accompanied by a major release of gas (CO_2 and H_2O) that occurs in temperature range of 200–400 °C (for urea and ammonium carbonate) and 350–450 °C (for oxalic acid), respectively. Ammonia and nitrous gases were also put in evidence.

Based on the FT-IR spectroscopy associated with thermal and gas evolved analyses, yttrium–aluminum-based precursors have the following general formulas: $M_2(C_2O_4)_3 \cdot a(NH_4)_2 C_2O_4 \cdot bM(OH)_3 \cdot cH_2O$ (oxalic acid), $M_2(CO_3)_3 \cdot aM(OH)_3 \cdot cM(NO_3)_3 \cdot dH_2O \cdot eNH_3$ (urea), and $M_2(CO_3)_3 \cdot aM(OH)_3 \cdot bH_2O$ (ammonium carbonate).

BET and SEM investigations were also used to illustrate changes related to the morphology and particle size for both precursors and YAG phosphors powders. As a general trend, a significant increase of pore diameter together with decrease of their volume was observed for all the precursors during the thermal treatment.

The photoluminescent spectra showed that the strongest emission band of Eu^{3+} changed from 594 nm when urea and ammonium carbonate was used as precipitating agents to 613 nm when oxalic acid was used.

Urea and ammonium carbonate lead to the formation of YAG type phosphors, with garnet structure and specific orange-red emission. Oxalic acid generates a non homogeneous powder that contains mostly Y_2O_3 Eu^{3+} together with $Y_3Al_5O_{12}$:Eu^{3+} and $Y_4Al_2O_9$:Eu^{3+} that explain the relative higher emission intensity.

References

1. Chen L, Lin CC, Yeh CW, Liu RS. Light converting inorganic phosphors for white light-emitting diodes. Materials. 2010;3(3): 2172–95.
2. Yen WM, Shionoya S, Yamamoto H. Practical application of phosphors. Boca Raton: CRC press; 2007.
3. Speghini A, Piccinelli F, Bettinelli M. Synthesis, characterization and luminescence spectroscopy of oxide nanopowders activated with trivalent lanthanide ions: the garnet family. Opt Mater. 2011;33(3):247–57.
4. Saladino ML, Caponetti E, Martino DC, Enzo S, Ibba G. Effect of the dopant selection (Er, Eu, Nd or Ce) and its quantity on the formation of yttrium aluminum garnet nanopowders. Opt Mater. 2008;31:261–7.
5. Yang H, Kim YS. Energy transfer-based spectral properties of Tb-, Pr-, or Sm-codoped YAG:Ce nanocrystalline phosphors. J Lumin. 2008;128:1570–6.
6. Lu J, Ueda K, Yagi H, Yanagitani T, Akiyama Y, Kaminskii AA. Neodymium doped yttrium aluminum garnet $Y_3Al_5O_{12}$ nanocrystalline ceramics-a new generation of solid state laser and optical materials. J Alloy Compd. 2002;341:220–5.
7. Li Y, Zhou S, Lin H, Hou X, Li W. Intense 1064 nm emission by the efficient energy transfer from Ce^{3+} to Nd^{3+} in Ce/Nd co-doped YAG transparent ceramics. Opt Mater. 2010;32(9): 1223–6.
8. Kyoung HY, Jong WC, Moon BK, Jeong JH, Jang K, Lee HS, Yi SS. Photoluminescence investigations of YAG:Eu nanocomposite powder by high-energy ball milling. Curr Appl Phys. 2009; 9(2):e86–8.
9. Zhou YH. Preparation of $Y_3Al_5O_{12}$:Eu phosphors prepared by citric-gel method and their luminescent properties. Opt Mater. 2002;20:13–20.
10. Lu CH, Jagannathan R. Cerium-ion-doped yttrium aluminum garnet nanophosphors prepared through sol–gel pyrolysis for luminescent lighting. Appl Phys Lett. 2002;80:3608–10.
11. Zhou YH, Lin J, Yu M, Han SM, Wang SB, Zhang HJ. Morphology control and luminescence properties of YAG:Eu phosphors prepared by spray pyrolysis. Mater Res Bull. 2003; 38(8):1289–99.
12. Yucai H, Yimin L, Xuehua Y, Li Z, Junsheng Y. Synthesis and characterization of YAG: Ce3+ fluorescence powders by co-precipitation method. J Rare Earths. 2010;28:303–7.
13. Katelnikovas A, Vitta P, Pobedinskas P, Tamulaitis G, Zukauskas A, Jøgensenc JE, Kareiva A. Photoluminescence in sol–gel-derived YAG:Ce phosphors. J Cryst Growth. 2007;304(2):361–8.
14. Yang ZP, Li X, Yang Y, Li XM. The influence of different conditions on the luminescent properties of YAG:Ce phosphor formed by combustion. J Lumin. 2007;122–123:707–9.

15. Ramanathan S, Kakade MB, Ravindran PV, Kalekar BB, Chetty KV, Tyagi AK. Thermal decomposition behavior of precursors for yttrium aluminum garnet. J Therm Anal Calorim. 2006; 84(2):511–9.

16. Marchal J, John T, Baranwal R, Hinklin T, Laine RM. Yttrium aluminum garnet nanopowders produced by liquid-feed flame spray pyrolysis (LF-FSP) of metalloorganic precursors. Chem Mater. 2004;16:822–31.

17. Popovici E-J, Morar M, Mureşan L, Grecu R, Barbu-Tudoran L, Indrea E. Study on the synthesis of cerium doped yttrium aluminate powders with luminescent properties. J Optoelectron Adv Mater Symp. 2009;1(6):1000–3.

18. Muresan L, Popovici E-J, Grecu R, Barbu Tudoran L. Studies on the synthesis of europium activated yttrium oxide by wet-chemical method. J Alloy Compd. 2009;471(1–2):421–7.

19. Durrani SK, Saeed K, Qureshi AH, Ahmad M, Arif M, Hussain N, Mohammad T. Growth of Nd-doped YAG powder by sol spray process. J Therm Anal Calorim. 2011;104:645–51.

20. Palmero P, Montanaro L. Thermal and mechanical-induced phase transformations during YAG and alumina-YAG synthesis. J Therm Anal Calorim. 2007;88(1):261–7.

21. Zhang HJ, Wang XJ, Jia QL, Sun HW. Artificial neural network analysis of preparation of nano a-Al_2O_3 powders by thermal decomposition of ammonium aluminium carbonate hydroxide. Mater Sci Technol. 2007; 23(9):1021–6.

22. Peng WS, Liu GK. Infrared spectra of minerals. Beijing: Science Press; 1982. p. 251 (In Chinese).

23. Su J, Zhang QL, Gu CJ, Sun DL, Wang ZB, Qiu HL, Wang AH, Yin ST. Preparation and characterization of $Y_3Al_5O_{12}$ (YAG) nano-powder by co-precipitation method. Mater Res Bull. 2005; 40:1279.

24. Hassanzadeh-Tabrizi SA. Low temperature synthesis and luminescence properties of YAG:Eu nanopowders prepared by modified sol–gel method. Trans Nonferr Met Soc. 2011;21:2443–7.

25. Wu X, Liang Y, Liu R, Li Y. The photoluminescence properties of Y_2O_3:Eu^{3+} prepared by surfactant assisted co-precipitation-molten salt synthesis. Mater Res Bull. 2010;45:594–7.

26. Yang HK, Chung JW, Moon BK, Jeong JH, Jang K, Lee HS, Yi SS. Photoluminescence investigations of YAG:Eu nanocomposite powder by high-energy ball milling. Curr Appl Phys. 2009;9: e86–8.

27. Liu FW, Hsu CH, Chen FS, Lu CH. Microwave-assisted solvo-thermal preparation and photoluminescence properties of Y_2O_3:Eu^{3+} phosphors. Ceram Int. 2012;38:1577–84.

28. Nissamudeen KM, Gopchandran KG. Y_2O_3:Eu^{3+} based nanophosphors with higher oscillator strength through lithium incorporation and indirect oxidation. J Alloy Compd. 2010;490: 399–406.

29. Jung HC, Park JY, Seeta G. Crystalline structure dependence of luminescent properties of Eu^{3+-} activated Y_2O_3–Al_2O_3 system phosphors. Curr Appl Phys. 2009;9:S217–21.

30. Muresan L, Popovici E-J, Indrea E. Structural and luminescence characterization of yttrium oxide based phosphors prepared by wet-chemical method. J Optoelectron Adv Mater. 2011;13(3): 183–9.

31. Ryba-Romanowski W, Lisiecki R, Rzepka A, Lipin'ska L, Pajączkowska A. Luminescence and excitation energy transfer in rare earth-doped $Y_4Al_2O_9$ nanocrystals. Opt Mater. 2009;31: 1155–62.